Available online at www.sciencedirect.com
ScienceDirect
Journal of Power Sources 174 (2007) 148–158
JOURNAL OF POWER SOURCES
www.elsevier.com/locate/jpowsour

Carbon nanotube supported Pt electrodes for methanol oxidation: A comparison between multi- and single-walled carbon nanotubes

Gang Wu [1], Bo-Qing Xu *

Innovative Catalysis Program, Key Lab of Organic Optoelectronics and Molecular Engineering, Department of Chemistry, Tsinghua University, Beijing 100084, China

Received 9 August 2007; accepted 9 August 2007
Available online 17 August 2007

Abstract

This work presents a detailed comparison between multi-walled (MWNT) and single-walled carbon nanotubes (SWNT) in an effort to understand which can be the better candidate of a future supporting carbon material for electrocatalyst in direct methanol fuel cells (DMFC). Pt particles were deposited via electrodeposition on MWNT/Nafion and SWNT/Nafion electrodes to investigate effects of the carbon materials on the physical and electrochemical properties of Pt catalyst. The crystalloid structure, texture (surface area, pore size distribution, and macroscopic morphology), and surface functional groups for MWNT and SWNT were studied using XRD, BET, SEM and XPS techniques. Cyclic voltammetry (CV) and electrochemical impedance spectroscopy (EIS) were employed to characterize the electrochemically accessible surface area and charge transfer resistances of the MWNT/Nafion and SWNT/Nafion electrodes. CO stripping voltammograms showed that the onset and peak potentials on Pt-SWNT/Nafion were significantly lower that those on the Pt-MWNT/Nafion catalyst, revealing a higher tolerance to CO poisoning of Pt in Pt-SWNT/Nafion. In methanol electrooxidation reaction, Pt-SWNT/Nafion catalyst was characterized by a significantly higher current density, lower onset potentials and lower charge transfer resistances using CV and EIS analysis. Therefore, SWNT presents many advantages over MWNT and would emerge as an interesting supporting carbon material for fuel cell electrocatalysts. The enhanced electrocatalytic properties were discussed based on the higher utilization and activation of Pt metal on SWNT/Nafion electrode. The remarkable benefits from SWNT were further explained by its higher electrochemically accessible area and easier charge transfer at the electrode/electrolyte interface due to SWNT's sound graphitic crystallinity, richness in oxygen-containing surface functional groups and highly mesoporous 3D structure.

Keywords: Electrocatalysis; Methanol oxidation; Catalyst support; Carbon nanotubes; Platinum

1. Introduction

Polymer electrolyte membrane fuel cells, such as hydrogen fueled proton exchange membrane fuel cells (PEMFC) and direct methanol fuel cells (DMFC) have been considered as promising low-temperature green power sources for automobiles, residence, and portable electronic devices [1–3]. Among many technical barriers to commercial applications of these fuel cells, the insufficient activity and durability of electrocatalysts are significant problems. Nanosized Pt seems to be the only effective catalyst in promoting the adsorption/dissociation of methanol in acid media. Many chemical approaches have been attempted to tailor Pt-based electrode catalysts to improve their activity, durability and Pt utilization in DMFC technology, including alloying Pt with other transition metals or promoting Pt with metal oxides, optimizing the composition, structure, size and shape of Pt-based nanoparticles. The electrochemical properties of Pt-based electrode catalyst are also significantly affected by the supporting carbon material, and the nature of supporting carbon materials can be crucial in determining the electrochemical performance of the electrode catalysts [4,5]. The key properties of being a suitable supporting material for electrocatalyst include electron conductivity, surface area, microstructure, macromorphology, corrosion resis-

* Corresponding author. Tel.: +86 10 62792122; fax: +86 10 62792122.
E-mail addresses: wugang@engr.sc.edu (G. Wu), bqxu@mail.tsinghua.edu.cn (B.-Q. Xu).
[1] Present address: Department of Chemical Engineering, University of South Carolina, Columbia, SC 29208, USA.

0378-7753/$ – see front matter © 2007 Elsevier B.V. All rights reserved.
doi:10.1016/j.jpowsour.2007.08.024

tance and cost. Carbon black Vulcan XC-72 has been the most widely used supporting material because of its reasonable balance among electron conductivity, surface area, and cost [6,7]. Thus, improvement and optimization of an electrocatalyst should include improvements both in the active metal (Pt) component and in the supporting carbon materials.

Due to their unique structure, high surface area, low resistance and high stability in electrochemistry [8,9], carbon nanotubes (CNTs) have been a main focus of many recent research efforts to seek alternative supporting carbon materials. The CNT materials are known in two types, i.e., single-walled (SWNTs) and multi-walled CNTs (MWNTs) that are consisting of a single and several graphite-layer in the wall of a tube, respectively [10–12]. The lengths of these CNTs are usually in the micrometer range with diameters vary from 0.4 to 3 nm for SWNT and from 1.4 to 100 nm for MWNTs. A number of earlier investigations have demonstrated that Pt-based electrocatalysts supported by properly pretreated MWNTs would show enhanced electrocatalytic activity for the reduction of oxygen at the cathode [13] and for the oxidation of CO [14] and methanol at the anode [15–17].

Attempts of using SWNTs as the supporting carbon materials also generated stimulating results [18–20]. In our earlier work [18], Pt nanoparticles deposited on SWNTs showed a remarkably enhanced activity for the electro-oxidation of methanol than those deposited on conventional Vulcan XC-72 carbon black. Kamat and co-workers [19,20] showed that in comparison with the assembly using Pt catalyst supported on commercial carbon black (CFE/CB/Pt), membrane-electrode-assembly (MEA) fabricated using SWNT supported Pt catalyst (CFE/SWNT/Pt) displayed significantly improved fuel cell performances in both hydrogen and methanol fuels. The maximum power density obtained using CFE/SWNT/Pt electrodes for anode as well as cathode was 20% higher than that obtained using CFE/CB/Pt electrodes in H_2/O_2 fuel cell. The methanol diffusion rate using CFE/SWNT/Pt electrodes was found threefold higher during methanol electrooxidation, which could be related to a ballistic diffusion occurring inside SWNTs [19]. Morover, a doping of small amount of SWNTs into traditional carbon or conductive polymers as composite catalyst support also led to a remarkable activity enhancement for the electrooxidation of methanol [21,22]. Quantitatively, a 10-fold increase in the catalytic activity of Pt/C was achieved by doping the catalyst with less than 2 wt% SWNTs. It was explained that the SWNT dopant functioned to increase the catalyst utilization by improving the interconnectivity among carbon black particles [22]. The activity enhancement of Pt electrocatalyt by doping with new carbon materials would be a very favorable approach for highly efficient and cost-effective electrocatalysis.

It is a surprising that the interest in potentials of CNT materials in the development of advanced electrocatalyst for the low-temperature fuel cells has been focused on either type of CNTs, namely SWNTs or MWNTs. Little is known about their difference in promoting the electrocatalysis of Pt-based electrodes. In this work, a side-by-side comparison between SWNTs and MWNTs has been made in terms of their physical and electrochemical properties. For the advancement of Pt electrocatalyst in DMFC technology, our motivation is to understand which of the two types of CNTs would be more functional as the supporting carbon materials.

2. Experimental

2.1. Materials pretreatments and preparations

The MWNT material (i.d. 3–10 nm, o.d. 6–20 nm, ratio of length to diameter 100–1000) was obtained from the laboratory of Professors Wei and Luo of the Chemical Engineering Department (Tsinghua University), where the material was prepared by catalytic vapor deposition (CVD) of propylene using Fe/Al_2O_3 as a catalyst and propylene as a carbon source [23]. The SWNT sample with diameters of 1.25 ± 0.2 nm and lengths between 1 and 10 μm was synthesized by arcing method [24] in Professor Chen's group of the School of Chemistry at Nankai University. For the deposition of Pt nanoparticles on CNT materials, an effective pretreatment method we practiced on raw CNT materials is the oxidation in a mixture of 70% HNO_3 + 98% H_2SO_4 solution (volume ratio 1:3) under refluxing at 80–90 °C for 1 h, followed by extensive washing with deionized water [14,22]. The same pretreatment was done on both SWNT and MWNT samples prior to any measurements in the present work.

To prepare SWNT/Nafion and MWNT/Nafion composite film electrodes, the pretreated MWNT and SWNT samples (8 mg) were first dispersed, respectively, in an isopropanol solution containing 5% Nafion (1 ml) under ultrasonic agitation (1 h). The suspension pastes were then applied by micropipette (15 μl) onto a glassy carbon-rotating disc electrode (GC-RDE) (diameter 5 mm). Morphologic structure of the MWNT/Nafion and SWNT/Nafion composites was characterized with scanning electron microscopy (SEM). And, the electrochemical properties of the MWNT/Nafion and SWNT/Nafion films coated on GC-RDE were measured with cyclic voltammograms (CV) and electrochemical impedance spectroscopy (EIS), details of which were described in the subsection of characterizations.

The Pt-loaded electrode samples were prepared by electrodeposition in 0.5 M H_2SO_4 solution containing 3 mM H_2PtCl_6, the working electrode was the GC-RDE coated with MWNT/Nafion or SWNT/Nafion films. The advantages of electrodeposition include uniform deposition of charged particles and control of film morphology by modulating the applied electric field [25,26]. Also, the loading of Pt in the electrodeposition can be accurately controlled by adjusting the electric charges. The steady state polarization curves were measured at first with a sweep rate of 2 mV s^{-1} in order to understand the cathodic behaviors of Pt electrodeposition onto the MWNT/Nafion and SWNT/Nafion electrodes. Then, Pt electrodeposition was conducted at −0.05 V for varying periods to change the Pt loadings in the range of 5–100 μg-Pt cm^{-2}. Although the loadings of Pt can be estimated by quantification of the total charges (current efficiency was assumed as 95% according to the polarization curves) during the electrodeposition, the actual Pt loadings were double checked later by atomic adsorption

spectrometry (AAS, Perkin-Elmer AA100) measurements. The Pt-loaded samples were denoted as Pt-MWNT/Nafion and Pt-SWNT/Nafion, respectively.

2.2. Characterizations

Surface areas and pore size distribution of the pretreated CNT materials were measured by nitrogen adsorption at 77 K on a Micromeritics ASAP 2010C instrument. The crystallinity of the carbon materials and their Pt loaded samples were characterized by X-ray diffraction (XRD) on a Bruker d8 diffractometer system equipped with a Cu Kα radiation and a graphite monochromatic operation at 45 kV and 40 mA. The diffraction patterns were obtained at a scan rate of $5^\circ\ min^{-1}$ with a step of 0.02°.

The sample morphology and metal dispersion were characterized by scanning electron microscopy (SEM) on a Hitachi S-5400 instrument and transmission electron microscopy (TEM) on a JEM-100S microscope operating at 150 kV. The samples were also analyzed by X-ray photoelectron spectroscopy (XPS) using an ESCA 210 and MICROLAB 310D spectrometer. Deconvolution and curve-fitting of the spectra were done using a VGX900 program.

Cyclic voltammograms (CV) characterization of the CNT/Nafion and Pt-CNT/Nafion coated GC-RDE was carried out between 0 and 1.2 V at a sweep rate of $20\ mV\ s^{-1}$. The electrochemical impedance spectroscopy (EIS) measurements of the samples were performed under open circuit potential with an excitation signal of 5 mV in the frequency range of 100 kHz and 0.1 Hz. The Zsimpwin fitting program was used to analyze the impedance parameters. An EG&G model 273 potentiostat/galvanostat and a Solarton 1025 Frequency Response Detector were used in the electrochemical measurements using a conventional three-electrode cell at room temperature ($23 \pm 2\ ^\circ C$). A SCE and a large-area Pt mesh electrode were used as the reference and the counter electrodes, respectively.

2.3. CO stripping and methanol electrooxidation

CO stripping measurements were conducted in 0.5 M H_2SO_4 solution [14]. The electrolyte solution was firstly purged with high purity nitrogen gas. Adsorption of CO on the electrode catalyst was conducted by bubbling a CO gas (UHP grade) through the electrolyte solution for 15 min, followed by purging with nitrogen for 20 min to remove any residual CO from the solution. The CO stripping CV curve and blank CV curve can be obtained from two consecutive scan cycles in the potential between 0 and 1.25 V at a sweep rate of $10\ mV\ s^{-1}$.

The methanol electrooxidation study over the Pt-MWNT/Nafion and Pt-SWNT/Nafion loaded with $100\ \mu g\text{-}Pt\ cm^{-2}$ were performed by CV and EIS measurements in 0.5 M CH_3OH + 0.5 M H_2SO_4 solutions at room temperature. The CV curves were recorded from 0 to 1.25 V at a sweep of $10\ mV\ s^{-1}$. The EIS measurement was conducted at a potential of 0.65 V in the frequency range between 100 kHz and 0.01 Hz, using an excitation signal of 5 mV by a Solarton 1025 frequency response analyzer. The impedance parameters were fitted and analyzed using the Zsimpwin program.

3. Results and discussion

3.1. Structural, surface and electrochemical properties of SWNT and MWNT materials

Fig. 1 shows comparisons of the XRD patterns, pore size distribution and SEM morphologies of the SWNT/Nafion and MWNT/Nafion electrodes. The peak at the angle (2θ) of 26.0° in Fig. 1(a) is associated with the (0 0 2) diffraction of the hexagonal graphite structure in the carbon materials. The much higher intensity of this peak for the SWNT sample than for the MWNT sample indicates a much higher graphitization degree or graphitic crystallinity of SWNT. The higher graphitization degree would be an important quality of supporting carbon materials to electrocatalyst since it induces higher electron conductivity and stronger electronic interaction with the loaded catalytic metal particles [27], which suggests that SWNT sample could a better supporting carbon material than MWNTs for electron transfer during electrochemical reactions.

Table 1 compares the texture properties of the SWNT and MWNT samples. Although the BET surface area of the SWNT sample ($129\ m^2\ g^{-1}$) is lower than the MWNT sample ($175\ m^2\ g^{-1}$), the S_{meso}/S_{BET} and V_{meso} data were found similar for both SWNT and MWNT samples. The pore size (diameter) distribution curves for both samples are plotted in Fig. 1(b). The SWNT sample clearly showed a much higher percentage of larger mesorpores with diameters of 10–100 nm. It has been reported [28] that chemisorption sites in SWNT aggregates can be categorized into two types, one is at the inner surfaces inside the SWNTs (tubing pores) and the other is at the outer surfaces of the SWNT bundles and grooves formed at the contact between adjacent SWNTs. The chemisorption sites in the latter category are unique in interaction with loaded catalytic metal particles. Rolison and her co-workers [29,30] proposed that the transport of small molecules in larger mesopores (10–100 nm) could approach the diffusion rate in an open space. It is likely that the much higher percentage of larger mesopores (10–100 nm) in SWNT material would facilitate the diffusion of molecules, reaction intermediates and/or reacting species that are involved in the catalytic electrooxidation of methanol.

In terms of electrode property, Nafion in the MWNT/Nafion and SWNT/Nafion samples functions as a medium for proton transfer and also as a binder to the CNT materials. The addition of Nafion to the carbon materials also help to simulate the working environment of the catalyst layer in a fuel cell. Therefore, the comparison between MWNT/Nafion and SWNT/Nafion electrode would be more informative than a comparison just between SWNTs and MWNTs themselves. Shown in Fig. 1(c) and (d) are the SEM images of MWNT/Nafion and SWNT/Nafion electrodes, respectively. In comparison with the dominant rope-like network of the MWNT/Nafion sample, the SWNT/Nafion sample is featured by a uniform porous morphology, in which the SWNT bundles are interlinked with Nafion in forming a porous three-dimensional (3D) structure that is rich in larger mesopores.

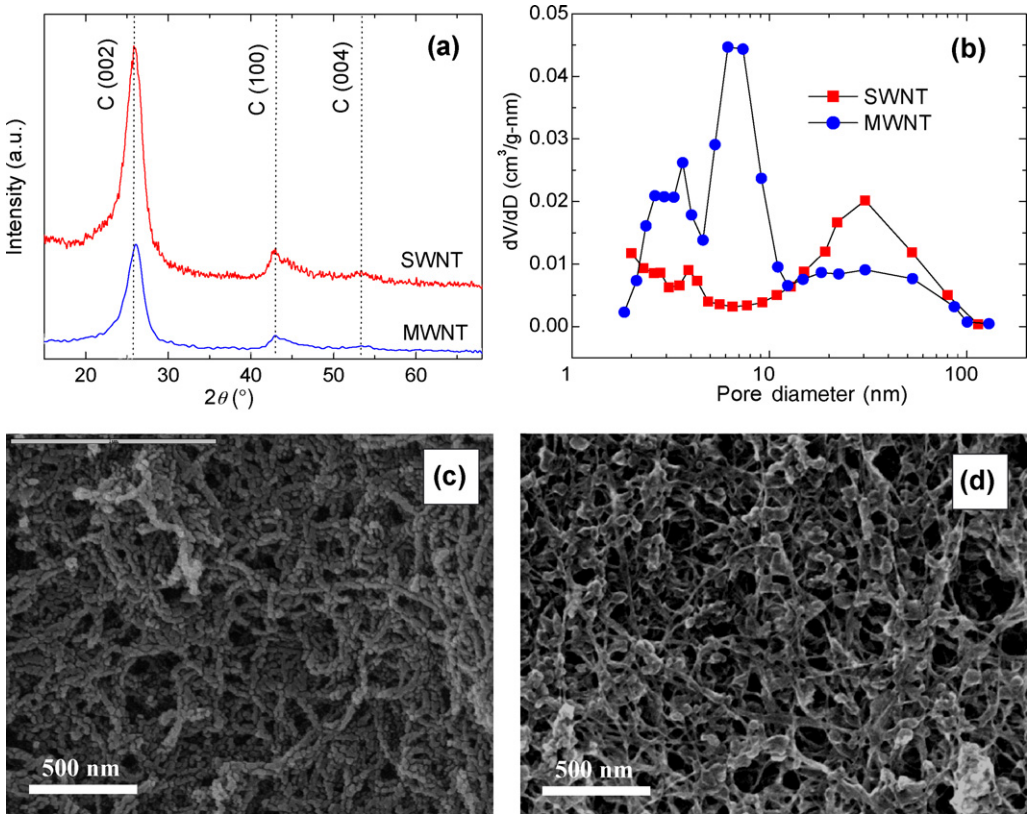

Fig. 1. X-ray diffraction (XRD) patterns (a) and pore size distribution curves (b) for MWNT and SWNT samples; SEM images of MWNT/Nafion (c) and SWNT/Nafion (d) electrodes.

It is understood that a continuous, 3D mesoporous structure is essential for promoting the transport of ions, fuel and solvent molecules in catalytic layer, which would benefit the deposition and accommodation of catalytic metal particles [30].

XPS measurements were made to characterize the surface states of the carbon materials. Fig. 2(a) and (b) shows the XPS spectra of C1s for the MWNT and SWNT samples, respectively. Three signals associate, respectively, with carbon atoms in graphitic (284.6 eV), –C–O like (285.8 eV) and high valence >C=O/–COO states (286.8 eV) were observed in the XPS spectra. By measuring the relative peak areas according to the curve-fitting, it was found that the percentage of carbon atoms in the oxygen-containing surface functional groups (–C–O, >C=O, –COO) was higher on the SWNT (18.8%) than on the MWNT sample (14.7%). In terms of a catalyst support, the higher concentration of the oxygen-containing surface functional groups at the SWNT surface would be a favorite for the subsequent deposition of Pt and for the supply of OH groups for the oxidation of CO and methanol [31]. We also recorded the O1s XPS spectra of the MWNT and SWNT samples, as shown in Fig. 2(c) and (d), respectively. These spectra can be deconvoluted into two major components. The component that shows the binding energy peak at around 532 eV is associated with surface C=O like species, and the other component with the binding energy peak at 533.5–535.5 eV can be assigned to other oxygen-containing surface functional groups. According to the curve-fitting, the percentage of the latter component on the SWNT sample (45.8%) was higher than that on the MWNT (38.7%) sample. Also, it is should be noted that the O1s binding energies in the SWNT sample were always higher than their counterparts in the MWNT sample, which indicates that the electrons of the oxygen atoms are bound more strongly with the surface carbons in the SWNT sample [32].

CV and EIS measurements were done to characterize the electrochemical properties of the MWNT/Nafion and SWNT/Nafion electrodes (Fig. 3). The voltammograms between 0.3 and 0.8 V in Fig. 3(a) can be regarded as an indicator of the electrode capacitive current that is dependent of the electrochemically accessible surface area of the electrode, S_a ($m^2\ g^{-1}$); i.e., the surface area of a porous electrode that can be accessed or reached by the

Table 1
Characteristics of both carbon nanotubes by N_2 adsorption/desorption: S_{BET}: BET surface area, S_{micro-}: micropore surface area, S_{meso-} mesopore surface area; V_{micro-}: micropore volume, V_{total}: total volume; V_{meso-}: mesopores volume; S_a electrochemically accessible surface area

CNTs	S_{BET} ($m^2\ g^{-1}$)	S_{micro-} ($m^2\ g^{-1}$)	S_{meso-} ($m^2\ g^{-1}$)	V_{total} ($cm^3\ g^{-1}$)	V_{micro-} ($cm^3\ g^{-1}$)	V_{meso-} ($cm^3\ g^{-1}$)	S_{meso-}/S_{BET}	S_a ($m^2\ g^{-1}$)
MWNT	175	26	149	0.38	0.011	0.37	0.85	52.5
SWNT	129	36	93	0.36	0.017	0.35	0.72	105.1

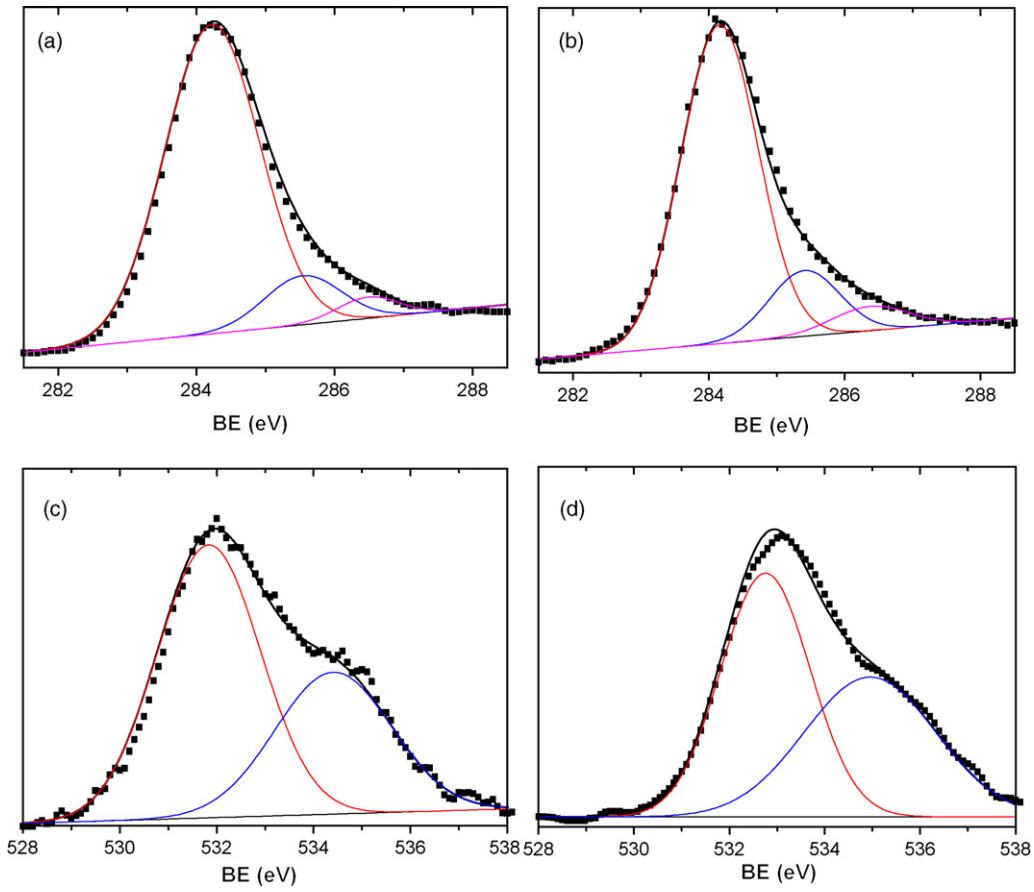

Fig. 2. C 1s core level XPS spectra of MWNT (a) and SWNT (b), and O 1s core level XPS spectra of MWNT (c) and SWNT (d).

electrolyte. The value of S_a can be obtained according to the equation: $S_a = C/C_{GC}$, where C is the gravimetric double layer capacitance ($F\,g^{-1}$) and C_{GC} is the double layer capacitance ($F\,m^{-2}$) of the glassy carbon electrode surface, for which a well accepted number is $C_{GC} = 0.2\,F\,m^{-2}$. The gravimetric double layer capacitance C ($F\,g^{-1}$) at a given sweep rate ν can be calculated according to measured current I and the electrode mass m using the equation: $C = I/\nu m$ [33]. The calculated S_a values are reported in the last column of Table 1, which shows that the electrochemically accessible surface area of SWNT/Nafion ($105.1\,m^2\,g^{-1}$) is twice that of the MWNT/Nafion electrode ($52.5\,m^2\,g^{-1}$). The S_a of SWNTs in the SWNT/Nafion electrode corresponded to 81.4% of their BET surface area (S_{BET}) but the S_a of MWNTs in the MWNT/Nafion electrode accounted only 29.9% of the surface of the incorporated MWNTs. The uniform and spacious larger mesoporous 3D structure of the SWNT/Nafion electrode and the presence of abundant oxygen-containing surface functional groups would be responsible for the much higher S_a in the SWNT/Nafion electrode [30,33]. The loss of surface area in the MWNTs for solvated ions in the electrolyte could indicate significant blocking by Nafion of the smaller pores in the MWNT/Nafion electrode.

Besides the electrochemical accessible surface area (S_a), charge (electron and proton) transfer is of great importance for methanol electrooxidation over Pt-based catalyst electrode containing a carbon support as the electron conductor and a Nafion binder as the proton conductor [34]. We carried out EIS measurement to understand the electrode structure and charge transfer properties in the MWNT/Nafion and SWNT/Nafion electrodes. The Nyquist plots at open circuit potential are shown in Fig. 3(b). Both electrodes display similar electrochemical impedance characteristics, namely, a depressed semi-circle in the high frequency region and a straight line at a slope of nearly 45° in the low frequency region, which are typical in the EIS of porous film coated on metals in an asymmetric metal/film/electrolyte configuration [35,36]. The depressed semi-circle in the high frequencies is ascribed to the charge (electron and proton) exchange at the carbon/electrolyte interface. The straight line at low frequencies can be expressed by adopting a Warburg diffusion element for the semi-infinite diffusion of ions at the carbon/electrolyte interface [35]. An equivalent circuit, shown as an inset in Fig. 3(b), is proposed to describe approximately the impedance behaviors of the present CNT/Nafion electrodes. In this equivalent circuit, R_{el} represents solution resistance; R_{ct}, charge transfer resistance; Q_{dl}, constant phase element (CPE); W, Warburg diffusion element; R_f, carbon resistance; C_f, carbon capacitance. Due to the porous nature of the supporting CNT materials, the double layer capacitance was expressed as constant phase element (CPE) Q_{dl} in the equivalent-circuit model. The CPE is defined as $Z_{CPE} = A(j\omega)^{-n}$, where A is the frequency-independent constant in capacitance and ω angular frequency; n is a correction factor between 0 and 1. The values

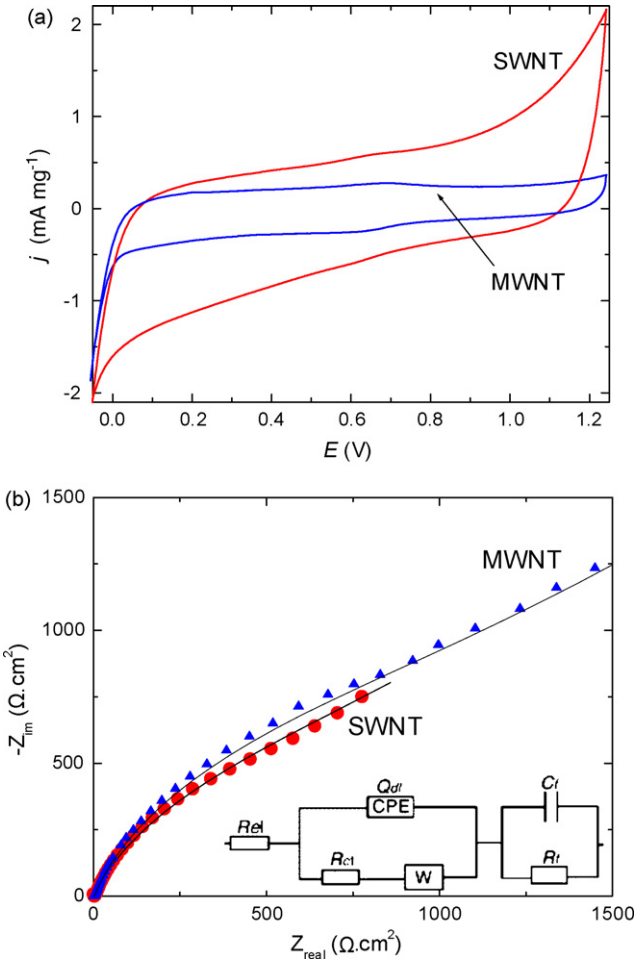

Fig. 3. Cyclic voltammograms (a) and Nyquist plots of EIS (b) for MWNT/Nafion and SWNT/Nafion electrode recorded in 0.5 M H_2SO_4. The inset of (b) is the equivalent circuit used for fitting the experimental data points; the solid lines show the fitted curves.

of Q_{dl} and n are related to the available porosity of the supporting CNT materials. The experimental results are shown as the data points and the fitted curves according to the equivalent circuit are plotted as solid lines in Fig. 3(b). Summarized in Table 2 are the impedance parameters that were used to produce the simulated fitting curves. In comparison with the MWNT/Nafion electrode, the SWNT/Nafion electrode was featured by higher CPE and a slight lower n values. In agreement with the preceding texture data, these features further demonstrate that the highly porous structure of the SWNT/Nafion electrode presents a higher percentage of surface area for electrochemical reactions. The SWNT/Nafion electrode showed also a significantly higher W and significantly lower R_{ct} (Table 2), which reveal a faster diffusion rate of solvated ions in its porous structure and a easier charge (electron and proton) transfer process

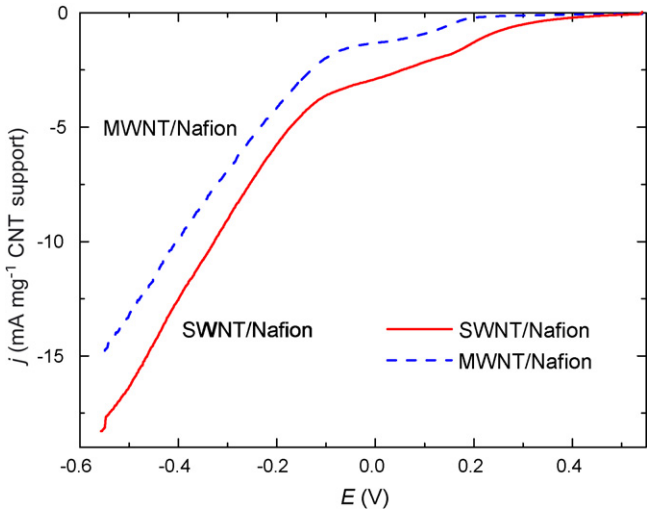

Fig. 4. Cathodic polarization curves for electrodeposition of Pt from 3 mM H_2PtCl_6 + 0.5 M H_2SO_4 solution on MWNT/Nafion and SWNT/Nafion electrodes at a sweep rate of 2 mV s^{-1} and rotating speed of 2000 rpm.

at the electrode/electrolyte interface during the EIS measurement. Moreover, the carbon paste resistance R_f was also lower in the SWNT/Nafion (0.48 Ωcm^2) than in the MWNT/Nafion (0.66 Ωcm^2) electrode, suggesting an enhanced electron conductivity in SWNT/Nafion electrode.

In summary, the above comparisons between our pretreated MWNT (MWNT/Nafion) and SWNT (SWNT/Nafion) samples in terms of structural, surface and electrochemical properties show that SWNT materials has a sound high degree of graphitization, a highly mesoporous 3D texture and possesses a higher concentration of oxygen-containing functional groups at its surface. In relation with these characteristics, the SWNT-containing electrode exhibits a higher electrochemically accessible surface area and faster charge transfer rate at the electrode/electrolyte interface.

3.2. Preparation and properties of Pt-loaded CNT electrodes

3.2.1. Electrodeposition of Pt on MWNT/Nafion and SWNT/Nafion electrodes

Electrochemical reduction of $[PtCl_6]^{2-}$ ions was conducted to further explore the influence of CNT materials on the properties of Pt electrocatalysts. Fig. 4 shows the cathodic polarization curves of Pt electrodeposition in 3 mM H_2PtCl_6 + 0.5 M H_2SO_4 solution on both SWNT and MWNT electrodes. These curves seem to indicate two consecutive reduction reactions in which Pt^{4+} and H^+ are reduced to Pt and H_2, respectively. The reduction of H^+ should occur more quickly than the reduction of

Table 2
EIS fitted parameters for MWNT/Nafion and SWNT/Nafion electrode in 0.5 M H_2SO_4 solution at open circuit potential

Electrodes	CPE × 10^5 (Ω^{-1} s^n cm^{-2})	n	R_{ct} (Ωcm^2)	$W \times 10^3$ (Ω^{-1} cm^{-2} $s^{0.5}$)	$C_f \times 10^6$ (F cm^{-2})	R_f (Ωcm^2)
MWNT/Nafion	146	0.81	1343	2.3	13	0.66
SWNT/Nafion	260	0.79	1074	3.1	37	0.48

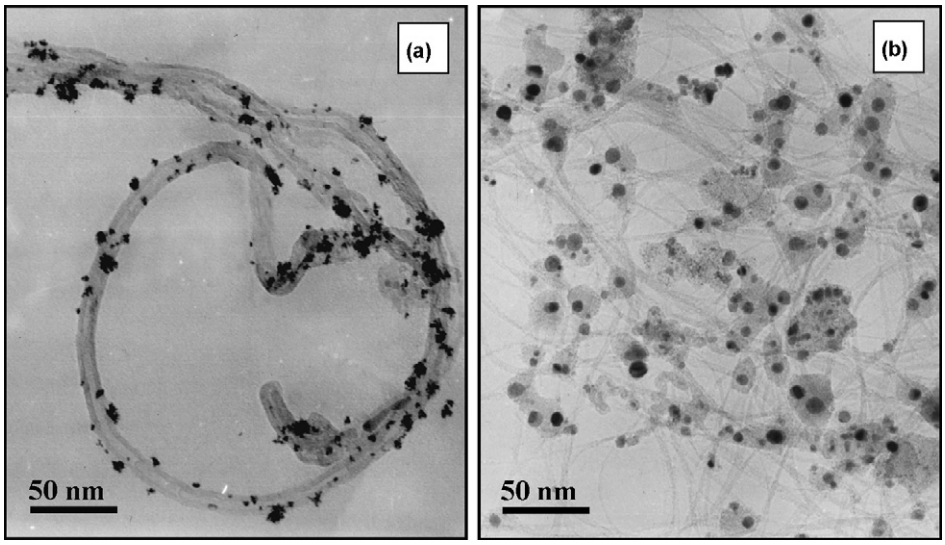

Fig. 5. TEM images of Pt-MWNT/Nafion(a) and Pt-SWNT/Nafion (b).

Pt when the reduction potential is lower than −0.15 V. The hydrogen evolution in these lower potentials would then significantly decrease the current efficiency, detrimentally affecting the electrodeposition of Pt. Hence, a potential of −0.05 V was chosen to electrodeposit Pt on both SWNT and MWNT electrodes, where the current efficiency can be as high as 95 percent. It should be noted that the electrodeposition of Pt on SWNT/Nafion yields always higher current than that on MWNT/Nafion at a given reduction potential, which can be attributed to the higher accessible surface area available in SWNT/Nafion for the deposition of Pt. In addition, the relatively positive onset potential for Pt reduction on SWNT/Nafion electrode indicates that the generation of Pt seeds on SWNT/Nafion is easier than on MWNT/Nafion, which may have relation with the unique mesoporous structure of SWNT/Nafion and the higher concentration of surface functional groups on SWNT [25]. By proper control of reaction time for Pt electrodeposition at −0.05 V, the loading of Pt was controlled in the range of 5–100 μg-Pt cm^{-2}.

3.2.2. *Properties of Pt-loaded MWNT/Nafion and SWNT/Nafion electrodes*

TEM micrographs for Pt-MWNT/Nafion and Pt-SWNT/Nafion having an identical loading of 100 μg-Pt cm^{-2} were presented in Fig. 5(a) and (b), respectively. As compared with Pt-MWNT/Nafion, Pt particles in Pt-SWNT/Nafion seemed to have closer contact with the network of entangled and branched bundles of SWNTs, and assumed shapes that are more close to highly exposed spheres. It is noteworthy that the Pt particles were anchored mainly at the boundaries of the SWNT bundles and Nafion binders, which would be highly favorable in the transport of electrons and protons during electrocatalysis. The beneficial morphology of Pt particles demonstrates again that the electrodeposition technique gives to higher utilization and more uniform dispersion of Pt particles [26].

For comparison, XRD patterns of Pt-MWNT/Nafion, Pt-SWNT/Nafion and E-TEK Pt/C catalysts are shows in Fig. 6. The diffraction peak at around 26.0° is associated with the C (0 0 2) planes in carbon supports. The peaks at 39.7, 46.2, 67.5 and 81.4° are characteristic diffraction peaks of face-centered cubic crystalline Pt (1 1 1), (2 0 0), (2 2 0) and (3 1 1) planes, respectively. In comparison with other Pt catalysts, Pt supported by SWNT/Nafion exhibited a relatively intense (1 1 1) plane. It was well understood that Pt-CO bonding at Pt (1 1 1) surface is weaker and CO electrooxidation potential at exposed Pt (1 1 1) facets is lower than those at Pt (1 0 0) facets [14,37]. Hence the preferential exposure of Pt (1 1 1) facets in Pt-SWNT/Nafion catalyst would help to enhance CO electrooxidation. The Pt (2 2 0) peak was selected to calculate the average Pt crystallite sizes according to the Debye–Scherrer formula [38], because it stands clear from the other diffraction peaks. The results indicated that Pt crystallites supported by MWNT/Nafion

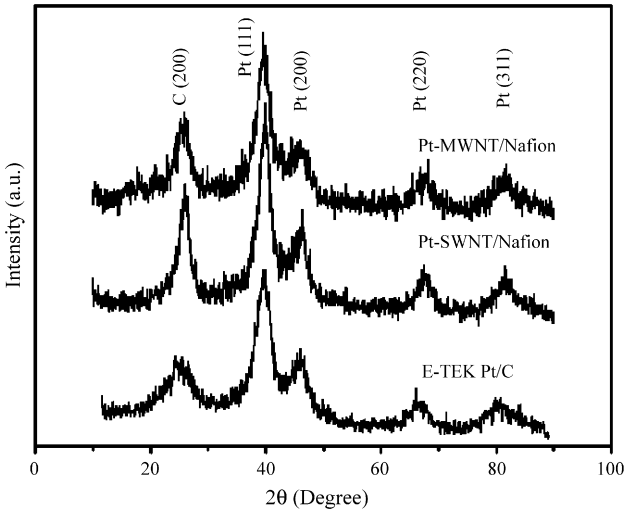

Fig. 6. XRD patterns of Pt-MWNT/Nafion, Pt-SWNT/Nafion and E-TEK Pt/XC-72.

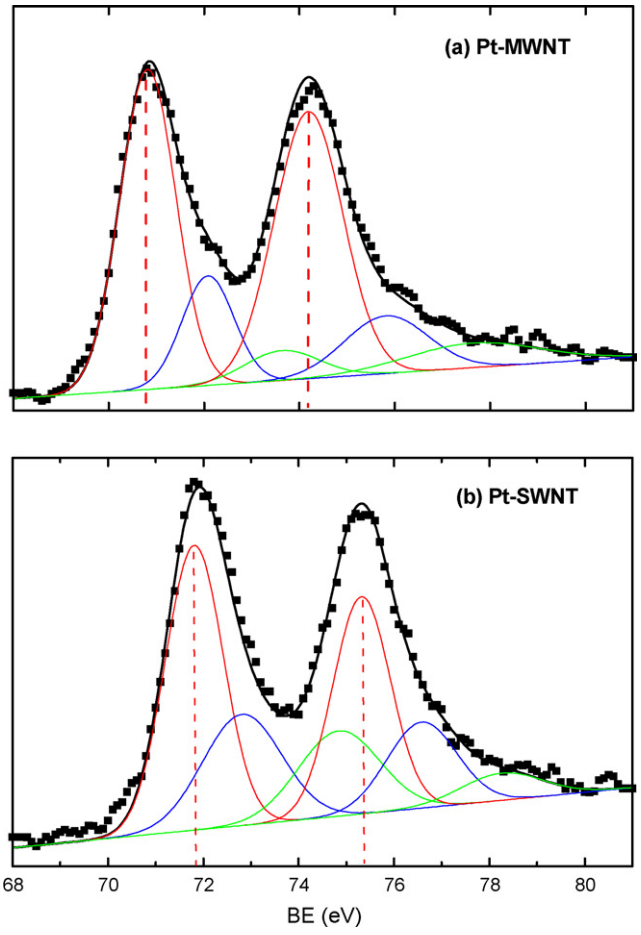

Fig. 7. The Pt 4f core level XPS spectra of Pt catalysts supported on MWNT/Nafion and SWNT/Nafion.

and SWNT/Nafion have similar average sizes, being 10.2 and 9.1 nm, respectively.

The Pt 4*f* signals in the XPS spectra of Pt-MWNT/Nafion and Pt-SWNT/Nafion consisted of three pairs of doublets, as shown in Fig. 7(a) and (b), respectively. According to the standard Pt 4*f* spectra [39], the most intense doublet peaks (near 71.1 and 74.4 eV) correspond to Pt in metallic state. Positive shifts in the metallic Pt(0) peaks toward higher binding energies (71.8 and 75.3 eV) were detected in the Pt-SWNT/Nafion catalyst when compared to Pt-MWNT/Nafion, probably due to stronger Pt-support interactions [32]. The second doublet (72.4 and 75.7 eV), which was observed at BEs 1.4 eV higher than that of Pt(0), could be assigned to the Pt(II) states in PtO or $Pt(OH)_2$. The third doublet of Pt was the weakest in intensity and showed even higher BEs (74.2, 77.7 eV), which is likely an indication for the presence of a very small amount of surface Pt (IV) species. It is worth noting that the percentage of oxidized Pt in Pt-SWNT/Nafion (45%) sample is higher than that in Pt-MWNT/Nafion (34%). According to the bifunctional mechanism of methanol electrooxidation, the higher percentage of oxidized Pt in Pt-SWNT/Nafion may enhance its electrocatalytic activity for methanol oxidation, by supplying OH groups at relatively lower potentials [36].

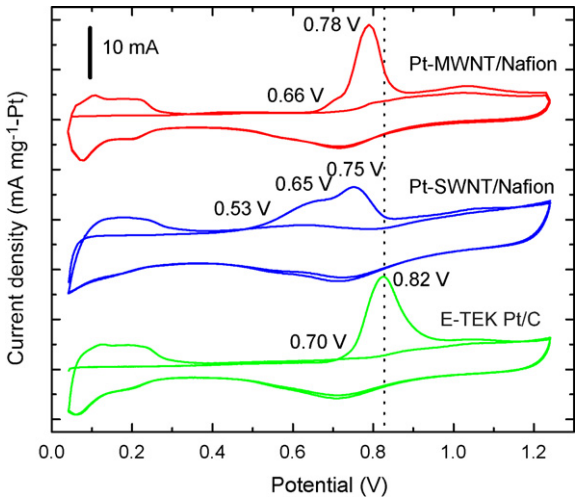

Fig. 8. CO stripping voltammograms over Pt-MWNT/Nafion, Pt-SWNT/Nafion and E-TEK Pt/XC-72 catalysts.

3.3. CO stripping study of Pt-MWNT/Nafion and Pt-SWNT/Nafion electrodes

Fig. 8 shows CO-stripping and background voltammograms of Pt-MWNT/Nafion and Pt-SWNT/Nafion catalysts in 0.5 M H_2SO_4 solution at a sweep rate of 10 mV s^{-1}. The voltammogram of an E-TEK Pt/C was also included for comparison. These data demonstrate that the onset potential of CO electrooxidation on Pt-SWNT/Nafion catalyst (0.53 V) is significantly lower than that of Pt-MWNT/Nafion (0.66 V), and both are lower than the onset potential of the E-TEK Pt/C catalyst (0.70 V). We have reported earlier [12] that small Pt nanoparticles loaded on MWNTs of different pretreatments by a modified colloidal method showed CO oxidation onset potentials that were 40–140 mV lower than that over a Pt/Carbon (Pt supported on Vulcan XC-72) synthesized using the same preparation, which resembles the commercial E-TEK Pt/C catalyst [40]. In principle, electrooxidation of CO occurs only when OH_{ad} forms on the surface of the Pt catalyst. The theoretical potential for the formation of OH_{ad} on Pt in acidic aqueous electrolyte solution is approximately 0.62 V at 25 °C [41]. Since the onset potential of CO electrooxidation is lower than 0.62 V on the present Pt-SWNT/Nafion catalyst, some active OH_{ad} groups or their equivalent might have been provided by the supporting SWNT, thereby partially explaining the decrease in onset potentials of CO oxidation on Pt-SWNT/Nafion when compared to Pt-MWNT/Nafion and conventional Pt/C catalysts.

Also, two well-separated CO oxidation peaks on Pt-SWNT/Nafion catalyst appear at 0.65 V and 0.75 V, both potentials are much lower than that of the single primary peak potential at 0.78 V on Pt-MWNT/Nafion catalyst, indicating that Pt-SWNT/Nafion is more tolerant to CO poisoning. These two CO oxidation peaks on Pt-SWNT/Nafion catalyst should be associated with two types of surface sites for CO adsorption. The presence of two types of Pt sites for CO adsorption was demonstrated by Becdelievre et al. [42], who discriminated the adsorbed CO species at the two types of Pt sites by reversing the potential sweep just before the appearance of

the second CO electrooxidation peak. The hydrogen adsorption/desorption signals on the subsequent potential sweep curve revealed that those adsorbed CO molecules associated with the second CO electrooxidation peak were blocking the Pt sites on which hydrogen atoms remained strongly adsorbed [42]. In other words, adsorbed CO molecules associated with the first CO electrooxidation peak (i.e., the one on the low potential side) would block the surface sites that adsorb hydrogen with relatively weak bonding. According to Beden and Lamy [37], the strength of hydrogen chemisorption on Pt sites depends on the structure of Pt surface. They also found that CO oxidation on single crystal Pt (1 1 1) surfaces occurs at a potential 50 mV lower than that on Pt (1 0 0) surfaces. Thus, the peak with the lower oxidation potential on the CO-stripping curve of the Pt-SWNT/Nafion catalyst could be associated with the electrooxidation of adsorbed CO molecules on the exposed (1 1 1) surfaces, whereas the peak with higher potential may be related with the oxidation of CO adsorbed on exposed (1 0 0) surfaces. This explanation is consistent with a preferential exposure of Pt (1 1 1) facets in Pt-SWNT/Nafion, as indicated in the XRD analysis.

Based on the electrochemically active area (ECA) and the specific activity (mA cm^{-2}) of the Pt catalysts, turnover frequency (TOF) of CO oxidation on surface Pt atoms at 0.65 V was calculated. The Pt-SWNT/Nafion catalyst appeared to show the highest TOF (0.023 s^{-1}) followed by the Pt-MWNT/Nafion (0.011 s^{-1}) and E-TEK Pt/C (0.003 s^{-1}). Quantitatively, the TOF rate on the Pt-SWNT/Nafion catalyst was twice that of Pt-MWNT/Nafion and eight times that of E-TEK Pt/C catalyst. The sound graphitic crystallinity and high density of surface functional groups on the SWNT support would be responsible for the high activity and higher tolerance to CO poisoning of the Pt-SWNT/Nafion catalyst since they could strengthen the metal-support interactions [43]. The concept that stronger metal-support interactions would benefit the electron transfer between the metal and support during the electrochemical reactions once was proven by an electron spin resonance (ESR) study [44].

The electrochemically active areas of Pt (ECA, $m^2\,g^{-1}$-Pt) as a function of Pt loadings for both Pt-SWNT/Nafion and Pt-MWNT/Nafion catalysts are compared in Fig. 9. It is clear that the ECAs of Pt-SWNT/Nafion catalysts are always higher than those of Pt-MWNT/Nafion at the Pt loading levels (5–100 μg cm^{-2}), indicating a higher utilization of Pt [45] on SWNT/Nafion support. The enhanced utilization of Pt can be partially accounted for by considering the unique morphology of Pt-SWNT/Nafion catalyst, in which highly exposed Pt particles are anchored mainly at the boundaries of the SWNT bundles and Nafion binders to benefit charge transfer.

3.4. Methanol electrooxidation on Pt-MWNT/Nafion and Pt-SWNT/Nafion electrodes

The typical CV curves for methanol electrooxidation over Pt-MWNT/Nafion and Pt-SWNT/Nafion catalysts with a loading of 100 μg-Pt cm^{-2} are shown as Fig. 10(a). The enhanced activity of Pt catalyst supported by SWNT/Nafion electrode is

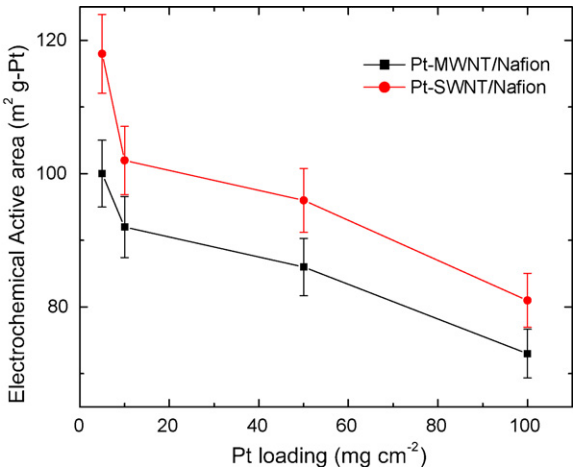

Fig. 9. Effect of Pt loading on the electrochemically active area of Pt in Pt-MWNT/Nafion and Pt-SWNT/Nafion electrodes.

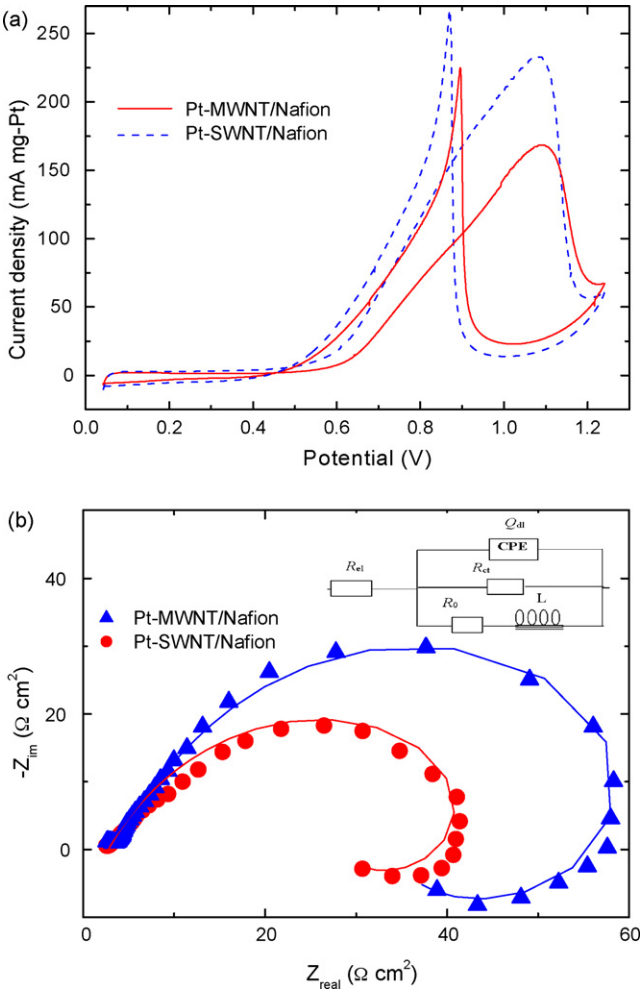

Fig. 10. Cyclic voltammograms (a) and Nyquist plots of EIS (b) for methanol oxidation over Pt-MWNT/Nafion and Pt-SWNT/Nafion catalysts (Pt loading: 100 μg cm^{-1}) in 0.5 M CH_3OH + 0.5 M H_2SO_4 solutions. The CV was recorded at a sweep rate of 10 mV s^{-1} and EIS was performed at 0.65 V.

evidenced by a slightly lower onset potential and significantly higher current density. The onset potential for Pt-SWNT/Nafion was 0.45 V while that for Pt-MWNT/Nafion was 0.50 V. In principle, with respect to the mechanism of methanol adsorption and dissociation on Pt sites, the onset potential is related to the breaking of C–H bonds and subsequent removal of CO_{ad} intermediates by oxidation with OH_{ad} supplied by Pt–OH sites or other sources. In our CO stripping measurements, the Pt-SWNT/Nafion electrode exhibited an enhanced activity in oxidizing adsorbed CO in comparison with Pt-MWNT/Nafion. In the similar way, the oxidative removal of C_1 intermediates would easily occur on Pt-SWNT/Nafion catalyst. Furthermore, stronger Pt-support interactions in the Pt-SWNT/Nafion catalyst would contribute more or less to the promotion of C–H breaking and CO_{ad} tolerance. Also, the significantly higher methanol oxidation currents in both forward and subsequently reversed scans for Pt-SWNT/Nafion catalyst clearly demonstrate a higher mass specific activity of Pt metal in Pt-SWNT/Nafion catalyst, due to the higher utilization of Pt (Fig. 9).

EIS measurements were carried out at 0.65 V to evaluate charge transfer property of methanol oxidation over Pt-MWNT/Nafion and Pt-SWNT/Nafion electrodes. The Nyquist plots are shown as Fig. 10(b). In our previous analysis of EIS for methanol oxidation over PtRu/C catalyst [46], the impedance behavior relating to the rate-determining step is dependent on the reaction potentials. At low potentials, methanol dehydrogenation was rate-determining step, whereas at high potentials, the oxidative removal of CO_{ad} became rate-determining step. Here, an intermediate potential (0.65 V), involved at the transition of rate-determining step from methanol dehydrogenation to oxidation of CO_{ad}, was chosen to compare the reactivity of Pt-MWNT/Nafion and Pt-SWNT/Nafion catalysts. As expected, the Nyquist plots were featured by an inductive loop in low frequency range for both Pt catalysts. The inductive loop in methanol electrooxidation indicates that the CO_{ad} coverage on Pt metal decreases with increasing the reaction potential ($b < 0$), and the decrease in CO_{ad} leads to an increase of Faradaic current ($m < 0$) [46]. A reasonable explanation for this observation is that enough OH_{ad} groups on Pt sites can be formed with increasing potential. The as-formed OH_{ad} groups are then used to oxidize CO_{ad} to decrease CO poisoning, generating more refreshed Pt sites for methanol adsorption to enhance the Faradaic current. Thus, an equivalent circuit representing the impedance behavior [46] is employed and shown as an inset in Fig. 10(b). The charge transfer resistances obtained from simulation of the impedance spectra were 58 and 36 Ωcm^2 for Pt-MWNT/Nafion and Pt-SWNT/Nafion catalysts, respectively, therefore proving much faster charge transfer rates during methanol electrooxidation on Pt-SWNT/Nafion catalyst.

4. Conclusions

This work provides a detailed comparison of MWNT and SWNT materials and elucidates the enhanced performance of SWNT as a novel supporting carbon material for electrocatalysts in DMFC. The SWNT is featured by a sound graphitic crystallinity and abundant oxygen-containing functional surface groups. The SWNT/Nafion composite electrode presents an interlinked highly mesoporous 3D structure with a higher electrochemically accessible surface area and easier charge transfer at the electrode/electrolyte interface. The unique structure was proven suitable for subsequent accommodation of catalytic metal (like Pt) particles and facilitates mass transfer (proton and methanol) during methanol oxidation.

Well-dispersed Pt particles were deposited on MWNT/Nafion and SWNT/Nafion electrodes by electrodeposition technique. Although the Pt particles exhibited similar average sizes on MWNT/Nafion and SWNT/Nafion electrodes, Pt particles deposited on the latter electrode assume sphere-like shapes and are anchored mainly at the boundaries of the SWNT bundles and Nafion binders, which are highly favorable for charge transfer (electrons and protons) during electrocatalysis. The unique morphology of Pt particles in the Pt-SWNT/Nafion catalyst also contributes to an improved utilization of Pt.

Lower onset and peak potentials in CO stripping voltammograms on Pt-SWNT/Nafion catalyst reveal a higher tolerance to CO poisoning on Pt, probably due to a better supply of reactive OH groups from the SWNT surface and a preferential exposure of Pt (1 1 1) facets in the catalyst structure. In methanol electrooxidation reaction, Pt-SWNT/Nafion catalyst exhibited a significantly higher current density, lower onset potentials and lower charge transfer resistances. Therefore, SWNT presents many advantages over MWNT and would emerge as an interesting supporting carbon material for fuel cell electrocatalysts.

Acknowledgements

The authors acknowledge the financial support for this work from NSF (Grant: 20590362), MOST (Grant: 2006AA03Z225) and Postdoctoral Science Foundation (2004035300) of China. We also appreciate Mr. Andrew Cavanaugh in the University of Maryland, Mr. Raja Swaidan in Cooper Union (NY) and Ms. Melanie Schaal in the University of South Carolina for their kind help in English.

References

[1] C. Cremers, M. Scholz, W. Seliger, A. Racz, W. Knechtel, J. Rittmayr, Fuel cells 7 (2007) 21.
[2] C. Coutanceau, R.K. Koffi, J.M. Leger, K. Marestin, R. Mercier, C. Nayoze, P. Capron, J. Power Sources 160 (2006) 334.
[3] L. Carrette, K.A. Friedrich, U. Stimming, Fuel cells 1 (2001) 5.
[4] V. Rao, P.A. Simonov, E.R. Savinova, G.V. Plaksin, S.V. Cherepanova, G.N. Kryukova, U. Stimming, J. Power Sources 145 (2005) 178.
[5] F.B. Su, J.H. Zeng, X.Y. Bao, Y.S. Yu, J.Y. Lee, X.S. Zhao, Chem. Mater. 17 (2005) 3960.
[6] K. Wikander, H. Ekstrom, A.E.C. Palmqvist, A. Lundblad, K. Holmberg, G. Lindbergh, Fuel Cells 6 (2006) 21.
[7] Z.L. Liu, L.M. Gan, L. Hong, W.X. Chen, J.Y. Lee, J. Power Sources 139 (2005) 73.
[8] M. Carmo, V.A. Paganin, J.M. Rosolen, E.R. Gonzalez, J. Power Sources 142 (2005) 169.
[9] A.L. Dicks, J. Power Sources 156 (2006) 128.
[10] T.W. Ebbesen, P.M. Ajayan, Nature 358 (1992) 220.
[11] S. Arepalli, P. Nikolaev, O. Gorelik, V.G. Hadjiev, H.A. Bradlev, W. Holmes, B. Files, L. Yowell, Carbon 42 (2004) 1783.

[12] Y. Li, X.B. Zhang, X.Y. Tao, J.M. Xu, W.Z. Huang, J.H. Luo, Z.Q. Luo, T. Li, F. Liu, Y. Bao, H.J. Geise, Carbon 43 (2005) 295.
[13] N. Rajalakshmi, H. Ryu, M.M. Shaijumon, S. Ramaprabhu, J. Power Sources 140 (2004) 250.
[14] L. Li, G. Wu, B.Q. Xu, Carbon 44 (2006) 2973.
[15] J. Prabhuram, T.S. Zhao, Z.K. Tang, R. Chen, Z.X. Liang, J. Phys. Chem. B 110 (2006) 5245.
[16] C.C. Chen, C.F. Chen, C.M. Chen, F.T. Chuang, Electrochem. Commun. 9 (2007) 159.
[17] A.L. Ocampo, M. Miranda-Hernandez, J. Morgado, J.A. Montoya, P.J. Sebastian, J. Power Sources 160 (2006) 915.
[18] G. Wu, Y.S. Chen, B.Q. Xu, Electrochem. Commun. 7 (2005) 1237.
[19] G. Girishkumar, M. Rettker, R. Underhile, D. Binz, K. Vinodgopal, P. McGinn, P. Kamat, Langmuir 21 (2005) 8487.
[20] G. Girishkumar, K. Vinodgopal, P.V. Kamat, J. Phys. Chem. B 108 (2004) 19960.
[21] G. Wu, L. Li, J.H. Li, B.Q. Xu, J. Power Sources 155 (2006) 118.
[22] J. Narayanamoorthy, S. Durairaj, Y. Song, Y. Xu, J. Choi, Appl. Phys. Lett. 90 (2007) 63112.
[23] Y. Wang, F. Wei, G.H. Luo, H. Yu, G.S. Gu, Chem. Phys. Lett. 364 (2002) 568.
[24] J. Chen, M.A. Hamon, H. Hu, Y.S. Chen, A.M. Rao, P.C. Eklund, R.C. Haddon, Science 282 (1998) 95.
[25] Z.D. Wei, S.H. Chan, J. Electroanal. Chem. 569 (2004) 23.
[26] G. Wu, L. Li, J.H. Li, B.Q. Xu, Carbon 43 (2005) 2579.
[27] K.W. Park, Y.E. Sung, S. Han, Y. Yun, T. Hyeon, J. Phys. Chem. B 108 (2004) 939.
[28] P. Serp, M. Corrias, P. Kalck, Appl. Catal. A 253 (2003) 337.
[29] D.R. Rolison, Science 299 (2003) 1698.
[30] M.L. Anderson, R.M. Stroud, D.R. Rolison, Nano Lett. 2 (2002) 235.
[31] R. Woods, J. Electroanal. Chem. 9 (1976) 1.
[32] A.S. Arico, A.K. Shukla, H. Kim, S. Park, M. Min, V. Antonucci, Appl. Surf. Sci. 172 (2001) 33.
[33] Y.K. Zhou, B.L. He, W.J. Zhou, J. Huang, X.H. Li, B. Wu, H.L. Li, Electrochim. Acta 49 (2004) 257.
[34] A. Havranek, K. Wippermann, J. Electroanal. Chem. 567 (2004) 305.
[35] L. Niu, Q.H. Li, F.H. Wei, X. Chen, H. Wang, J Electroanal. Chem. 544 (2003) 121.
[36] A. Tarola, D. Dini, E. Salatelli, F. Andreani, F. Decker, Electrochim. Acta 44 (1999) 4189.
[37] B. Beden, C. Lamy, Electrochim. Acta 35 (1990) 691.
[38] M. Kima, J.N. Park, H. Kima, S. Songa, W.H. Lee, J. Power Sources 163 (2006) 93.
[39] F. Sen, G. Gokagac, J. Phys. Chem. C 111 (2007) 5715.
[40] L. Li, H.X. Wang, B.Q. Xu, J.L. Li, W. Xing, Z.Q. Mao, Acta Phys. Chim. Sin. 19 (2003) 342.
[41] H.B. Zhang, G.D. Lin, Z.H. Zhou, X. Dong, T. Chen, Carbon 40 (2002) 2429.
[42] A.M. de Becdelièvre, J. de Becdelievra, J. Electroanal. Chem. 294 (1990) 97.
[43] Y. Nagai, T. Hirabayashi, K. Dohmae, N. Takagi, T. Minami, H. Shinjoh, S. Matsumoto, J. Catal. 242 (2006) 103.
[44] J.J. Baschuk, X. Li, Int. J. Energy Res. 25 (2001) 695.
[45] D. Zhao, B.Q. Xu, Angew. Chem. Int. Ed. 45 (2006) 4955;
D. Zhao, B.Q. Xu, Phys. Chem. Chem. Phys. 8 (2006) 5106.
[46] G. Wu, L. Li, B.Q. Xu, Electrochim. Acta 50 (2004) 1.